RESEARCH ARTICLE

A local magnitude scale for a volcanic region: the Canary Islands, Spain

Juan Rueda[1,2,3] · Julio Mezcua[3]

Abstract

In this study, we define a local magnitude scale for earthquakes occurring in the Canary Islands during the 2003–2020 period. We used data corresponding to 696 earthquakes (excluding those associated with the 2011–2015 El Hierro eruption), which consisted of 9267 observations in a hypocentral distance in the range of 10–500 km. Amplitudes were obtained by deconvolving the original recordings with the instrument response and then convolving the recording with the Wood-Anderson response. The amplitudes were inverted simultaneously to obtain the distance correction terms and station corrections. We found that the amplitude for this set of data is linearly attenuated. However, this is not the case for the seismicity recorded during the 2011 El Hierro eruption, which is the reason for excluding data for that case. We obtain a local magnitude of $M_L = \log A + 0.967 \log (R/40) + 0.00142 (R - 40) + 2.445 + S$, where A is the maximum amplitude in millimeters of the S wave for the horizontal components of the simulated Wood-Anderson instrument (WA), R is the hypocentral distance in kilometers, and S is the station correction for each component at every station. This relationship indicates that seismic waves at this island volcano setting are less attenuated than those in crustal continental settings, such as across the Iberian Peninsula or in California.

Keywords Canary Islands · Seismic attenuation · Local magnitude · Station corrections

Introduction

The most widely used estimate of earthquake size is the local magnitude (M_L) that was originally defined for California by Richter (1935) and is used by most earthquake catalogs (e.g., Langston et al. 1998; Ristau et al. 2016), including those maintained for volcanic systems (e.g., Del Pezzo and Petrosino 2001; D'Amico and Maiolino 2005; Pechmann et al. 2007). The ease of its calculation and the clear interpretation of the wave amplitude behavior with distance in terms of attenuation are determinants of the success of this scale

(e.g., Kiliç et al. 2017; Yenier 2017; Muñoz Lopez et al. 2020). The importance of calculating an M_L for a particular region is twofold: it enables the quantification of seismic wave attenuation with distance, and it is the best parameter for measuring seismic activity in any region (Richter 1958; Kanamori and Jennings 1978; Hutton and Boore 1987; Boore 1989). Other magnitude scales provide information on the moment of seismic releases, such as the moment magnitude (M_w). This parameter is intimately related to the physics of an earthquake, but it requires more elaborate processing, and this prevents its use in real-time. For this reason, we aim, here, to develop an M_L scale applicable to earthquakes at the Canary Islands (Spain), which can be used for real-time monitoring, especially during volcanic unrest (e.g., D'Amico and Maiolino 2005; Scordilis et al. 2013; Ristau et al. 2016; Condori et al. 2017).

Techniques for determining the magnitudes of earthquakes that occur on the Canary Islands have evolved since the installation of the first seismometers in 1952, as reviewed by Rueda et al. (2020). Since 2005, events with magnitudes of greater than four have been studied in almost real time, and full moment tensor inversion has been applied to obtain the moment magnitude (Rueda and Mezcua 2005).

✉ Juan Rueda
juanjose.rueda@upm.es

1 ETSI Topografía, Geodesia y Cartografía, Departamento de Ingeniería Topográfica y Cartografía, Universidad Politécnica de Madrid, Calle de la Arboleda s/n, 28031 Madrid, Spain

2 Instituto Geográfico Nacional, Calle General Ibáñez de Ibero 3, 28003 Madrid, Spain

3 Fundación José García Siñeriz, Calle Alenza 1, 28003 Madrid, Spain

To standardize the magnitude values, Rueda et al. (2020) proposed several relationships between the different scales which has been used in the Canary Islands and the moment magnitude. This results in a homogeneous magnitude catalog used recently for a seismic probabilistic hazard study (Mezcua and Rueda 2021). This new catalog is of great value for hazard studies, given that the seismic activity considered is from approximately $M_w = 3.5$ to the greatest magnitudes that correspond to historical events. However, we believe that in a volcanic area such as this, where episodes of generally low-magnitude seismic activity frequently occur, a better definition of parameters is needed to more precisely characterize the M_w required. These parameters include the b-value of the Gutenberg Richter recurrence law and its statistics, energy release, and a quantifiable traffic light system for hazard assessment based on earthquake magnitude (De la Cruz-Reyna and Tilling 2008).

The beginning of the instrumental period on the Canary Islands dates back to the installation of a network of three stations in 1975, although a single seismic station had been operating on Tenerife (in the Canary Islands) since 1952. However, after several earthquakes, including the widely felt earthquake of 1989 (Mezcua et al. 1992), the volcanic-related seismic crisis of 2003–2004 on Tenerife (Domínguez Cerdeña et al. 2011) and the 2011 El Hierro eruption (López et al. 2017), concerted efforts were made by the Spanish Instituto Geográfico Nacional (IGN) to increase the number of seismic stations on the islands, such that by 2021 more than 55 stations were in operation.

The main purpose of this paper is thus to develop a new M_L scale for the Canary Archipelago, based on Richter's (1935) definition, using the large data set generated by the broadband and short-period stations operating on these volcanic islands. Similar approaches have been applied previously for numerous other countries (Kavoura et al. 2020). Consequently, the main aims of this paper are to analyze the seismic wave attenuation for the Wood-Anderson amplitudes on the different islands of the archipelago and to assess the station corrections that need to be applied for the routine determination of magnitudes. Given that the attenuation parameters obtained for the M_L are highly dependent on tectonic conditions (which, in our case, correspond to an active oceanic volcano island chain), no attempt was made to employ the original formula obtained for southern California (Richter 1935) or any other M_L developed for other dissimilar tectonic environments.

## Seismotectonics and the structural properties of the Canary Islands

The islands of the Canary archipelago in the North Atlantic are aligned in an almost perfect E–W direction (Fig. 1). Their associated volcanic activity increases in age from west to east, with the oldest volcanic rocks found on the island of Fuerteventura (20.6 Ma) and the youngest on the islands of El Hierro (1.12 Ma) and La Palma (1.77 Ma) (Carracedo et al. 1998). This has led to the creation of a complex crustal structure beneath the islands chain, and also beneath individual islands and within single volcanoes (Banda et al 1981; Dañobeitia and Canales 2000; Carracedo and Troll 2016).

Seismic refraction studies carried out in the Canary Islands have revealed the existence of pure oceanic crust with a thickness of less than 10 km (Banda et al. 1981) and a Moho depth of 15 km under the islands of Fuerteventura, Gran Canaria, and Tenerife, but of only 11 km under Lanzarote (Martinez-Arevalo et al. 2013). The seismic velocities under the volcanic edifices provide no evidence of a common basement for all of the islands (Banda et al. 1981). The central and eastern islands have a 7–12 km deep crust with a high P wave velocity (almost 8 km/s), which has been interpreted as an indication of magmatic underplating (Dañobeitia and Canales 2000). This model has also been extended to the islands of Lanzarote and La Palma (Lodge et al. 2012).

Attenuation studies of the Canary archipelago have been conducted using coda waves (Canas et al. 1995, 1998; Núñez 2017) and by studying the scattering of P waves on Tenerife (García-Yeguas et al. 2012; Prudencio et al. 2013). The main conclusions for the archipelago as a whole are that the seismic attenuation for crustal earthquakes is not well defined: an NNW-SSE-oriented strip to the south of El Hierro has a low-quality factor parameter, Q_0, of 70–130, but there are also two areas to the north and south of this barrier that have a higher Q_0 of 210. For subcrustal earthquakes, high Q_0 values (> 180) have been detected between Gran Canaria and Tenerife and to the northeast of El Hierro (Núñez 2017). Studies focusing on Tenerife show a central area with high degrees of attenuation at depths of 6–10 km, which is possibly associated with magmatic underplating, but low attenuation in the external parts of the island (Prudencio et al. 2013). Of special relevance is the presence of a rigid vertical body between Tenerife and Gran Canaria defined by a relatively low Gutenberg–Richter b-value of 0.5 to 0.8 and surrounded by more plastic material with b-values greater than one. This structure is a very active seismic focus that reaches a depth of 60 km (Mezcua and Rueda 2021). Furthermore, in southwestern Tenerife, there is a volume with a radius of 6–8 km that is 10 km below the surface with a very high b-value of approximately two. This volume is possibly a partially depleted magma chamber (Mezcua and Rueda 2021).

A revised seismicity map of the Canary Islands for events of $M_w \geq 3.0$ has been drafted based on (1) the unified magnitude M_w for the years up to 2000 taken from Rueda et al. (2020), and (2) the seismicity provided by the IGN catalog (IGN 2021) and converted to moment magnitudes for
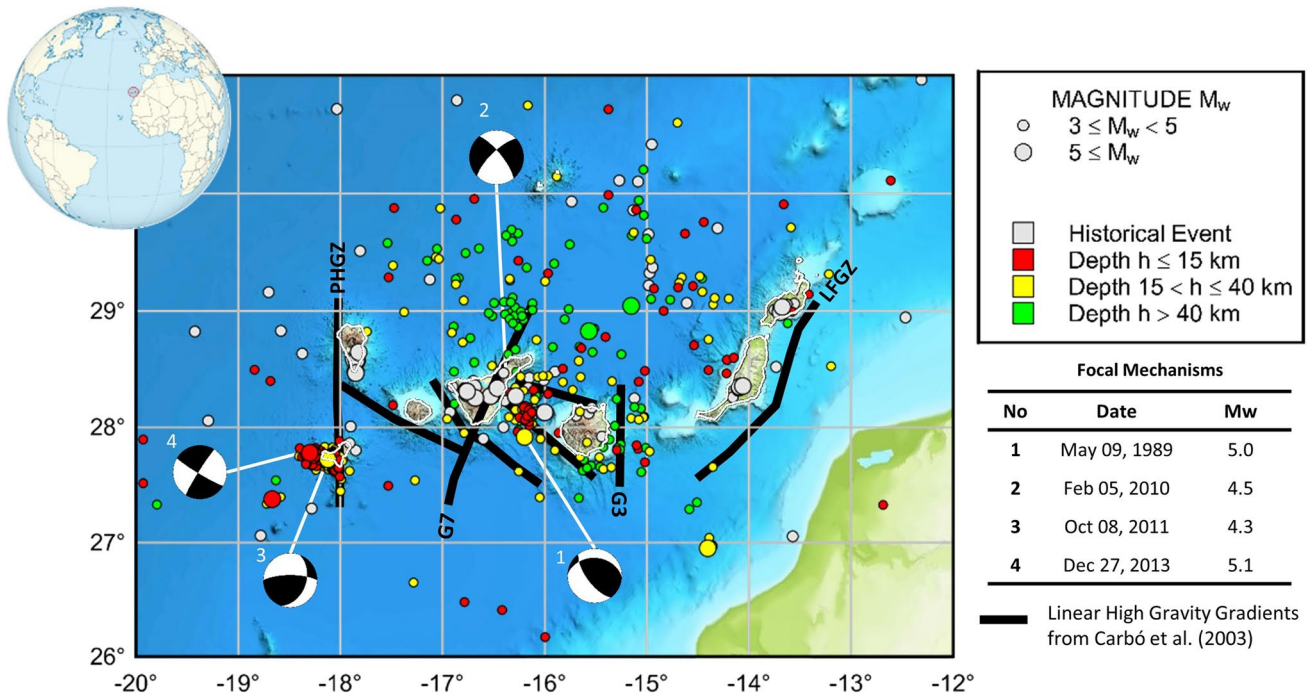
Fig. 1 Seismicity map for the Canary Islands of moment magnitudes (M_w) greater than 3 in the period of 1341–2020 taken from Rueda et al. (2020). The high linear gradients from Carbó et al. (2003) and the focal mechanisms of Mw > 4 are taken from the Global Centroid-Moment-Tensor Project (Dziewonski et al. 1981; Ekström et al. 2012)

(solutions 1, 2, and 4) and IGN (2021) for solution 3. Topographic and bathymetric data are from the National Geographic Institute, the Oceanography Spanish Institute, and the Navy Hydrographic Institute of Spain

the 2001–2020 period (Fig. 1). The main fractures in the Canary Islands and the surrounding ocean floor detected by geophysical, petrographic, and geochemical methods can be classified into two types of families, namely, Atlantic and African, depending on their relationship with the opening of the Atlantic or the tectonics of the African Atlas range on the African continent (Anguita and Hernán 1975; Fúster 1975; Carracedo 1984; Emery and Uchupi 1984; Dañobeitia 1988). In the African family of fractures, orientations are ENE-WSW and NNE-SSW, while for the Atlantic family, they are WNW-ESE. An offshore gravity study of the Canary Islands (Carbó et al. 2003) also revealed linear high-gravity gradients, as deduced from the short-wavelength Bouguer anomaly map. This indicates the presence of the tectonic structures near the surface depicted in Fig. 1.

Due to the low magnitude of the recorded earthquakes, the state of stress deduced from focal mechanisms offers four solutions for the Canary Islands area using moment tensor inversion. Composite focal mechanisms have been determined using P-wave polarities for some low-magnitude earthquakes registered on Tenerife (Mezcua et al. 1990), as well as for those derived from the 2011 seismo-volcanic crisis on El Hierro (del Fresno 2016). The only significant earthquakes that could be used for this purpose are shown in Fig. 1. This involves a total of four

usable events hereafter termed earthquakes 1 through 4. For the focal mechanism of "earthquake 1," which corresponds to the largest earthquake in the area during the period for which records are on hand, two solutions are available. These are, one taken from the Global Centroid Moment Tensor Project (Dziewonski et al. 1981; Ekström et al. 2012), which gives a depth of 15 km, and the other from Mezcua et al. (1992), which gives a depth of 25 km. Despite the differences in terms of focal depth, these solutions agree on the trend of the B-plane, e.g., approximately 290°, and the pressure axis, which is interpreted to be acting nearly horizontally. Because, as this event lies within the seismicity cluster, no geodynamic differences are apparent regardless of the chosen solution since the corresponding fault is confined inside the same rigid body. The solution for the very shallow earthquake 2 at a depth of 3 km and as obtained from the Global Centroid Moment Tensor Project (Dziewonski et al. 1981; Ekström et al. 2012) lies outside the seismicity cluster between Tenerife and Gran Canaria. However, one of its focal planes coincides with one of the gravimetric lineaments of the Atlantic family. The other two earthquakes, 3 (IGN 2021) and 4 (Global Centroid Moment Tensor Project (Dziewonski et al. 1981; Ekström et al. 2012)) are clearly associated with the seismic crisis related to the

2011 El Hierro eruption (del Fresno 2016); thus, tectonic inferences are restricted to this specific area.

Development of a magnitude definition using the catalog of seismic events for the Canary Islands

Although the first seismic station in the Canary Islands was installed in 1952, the magnitudes available for large earthquakes ($M_w > 4.5$) correspond only to those registered by international monitoring agencies through 1975. In 1975, a local seismic network with three telemetered stations was installed by IGN, began producing monthly local bulletins. The magnitude assignment for the network during 1975–1995 was calculated as the duration magnitude M_d following Lee et al. (1972):

$$M_d = -0.87 + 2.0\log(\tau) + 0.0035\Delta \tag{1}$$

where τ is the event duration in seconds and Δ is the epicentral distance in km from each station. However, during 1975–1987, an incorrect distance coefficient of 0.00035 was erroneously used in the place of the correct coefficient 0.0035, but this was later corrected; a correction that was included in the final catalog (Rueda et al. 2020).

During the 1996–2002 period, the $m_b(Lg)$ magnitude scale developed for the Iberian Peninsula was used. This applies for epicentral distances $\Delta < 3°$ and is given by Mezcua and Martínez Solares (1983) as:

$$m_b(Lg) = \log(A/T) + 1.05\log\Delta + 3.90 \tag{2}$$

where A is the sustained ground-motion amplitude of the S crust guided wave (Lg) in microns (S wave in the Canary Islands because of the lack of the granitic layer), and T is the period in seconds.

In addition, for events recorded on both the Iberian Peninsula and in the Canary Islands, for earthquakes in which the S wave was not fully developed, the m_b derivation of Veith and Clawson (1972) was used:

$$m_b = \log(A/T) + P(\Delta, h) \tag{3}$$

Here, A is the ground-motion amplitude of the P wave in microns, T is the period in seconds, and $P(\Delta, h)$ is a correction factor based on earthquake epicentral distance Δ from the sensor and depth h. This criterion was maintained until 2016.

In 2002, López (2008) derived a local magnitude expression for Iberia using the Spanish National Network. This was

$$M_L = \log A + 0.985\log(R/100) + 0.000993(R - 100) + 3.0 + S \tag{4}$$

Here, A is the maximum trace amplitude in millimeters measured on the output velocity instrument, as filtered to ensure that the response of the seismograph/filter system replicates that of a standard Wood-Anderson (WA) displacement seismograph. In addition, R is the hypocentral distance in km, and S is the station correction. This expression was considered to be applicable to both the Iberian Peninsula and the Canary Islands. Unfortunately, due to problems encountered with calculating the simulated Wood-Anderson amplitude, this magnitude formula was not used on a routine basis for Spanish seismicity (López 2008). For this reason, López (2008) suggests a magnitude expression that considers the amplitude of the ground and period measured directly from the velocity seismogram:

$$m(Lg) = \log(A/T) + 1.17\log R + 0.67 \tag{5}$$

In this expression, A is the ground-motion amplitude of the maximum of the S wave in microns, T is the period in seconds, and R is the hypocentral distance in km. Finally, between 2004 and 2022, for earthquakes with magnitudes greater than four, a moment magnitude value was obtained by moment tensor inversion, as described by Rueda and Mezcua (2005).

This derived magnitude expression—which is not a rigorous local magnitude—is, in fact, similar to the Richter definition. That is, they involve an attenuation correction for the distance traveled by the seismic wave that ensures that the resulting value is the same as the corresponding local magnitude if the period of the S wave is one second. However, when applying Eq. (5) to the Canary Archipelago, two problems arise:

(1) the attenuation terms for the Iberian region are expected to be different from those obtained on an oceanic volcanic area, and
(2) this expression uses not only the maximum amplitude but also the period, which means that this magnitude cannot be regarded as a local magnitude and so should be named m(Lg).

Moreover, as López (2008) pointed out, the magnitude values obtained with this expression for m(Lg) coincide with the local magnitude definition M_L (Eq. 4) deduced from López (2008) if the period of the wave is 1 s. However, the resulting value deviates, producing an error if more than 0.8 units of magnitude given that the period is less or greater than 1 s in the interval of 0.1–10 Hz. In short, the magnitude formula $m(Lg)$ derived by López (2008) for the Iberian Peninsula is not a real local magnitude, and its period dependence complicates its association with the local magnitude M_L also developed for Iberia by López (2008). The difference between the values provided by this expression and those that generate a local magnitude definition are especially important for local seismicity registered at short distances.

We thus believe that the discrepancy between the magnitude $m(Lg)$, which is considered standard in the catalog, and the true

local magnitude M_L, which is also defined by López (2008), may lead to serious distortions in the series of magnitudes. Consequently, in this paper, we aim to derive a new local magnitude definition, M_L, which is designed specifically for seismicity of the Canary Islands, thereby also producing a blueprint as to how this can be achieved on other seismically active volcanic islands.

Methods and data

The first successful measurement of the magnitude of an earthquake corresponds to the definition of the local magnitude, M_L, by Richter (1935), as based on measurements of the maximum amplitude A in mm, as recorded by a Wood-Anderson instrument with a free period (T) 0.8 s, a magnification of 2800 and damping of 0.8. The expression thus obtained was (Richter 1935):

$$M_L = \log A - \log A_0 + S \tag{6}$$

where A_0 is the distance correction term, S is a specific station correction for the M_L calculated by each station, and was a correction that was not considered in Richter's original paper.

Typically, two methods are used to obtain the values of $-\log A_0$. The first is the nonparametric method as introduced by Savage and Anderson (1995) and which employs the empirical distance correction $-\log A_0$ as determined by the data itself, but which includes no associated physical expression for the mechanism of the attenuation. As part of the approach, an empirical set of $-\log A_0$ terms are obtained by inverting Eq. (6) over an epicentral distance range, provided that enough data are available. An interpolation of these values generates a continuous $-\log A_0$ distribution for every epicentral/hypocentral distance. The second method uses the parametric model of Bakun and Joyner (1984) in which $-\log A_0$ has a physical interpretation. This approach considers several effects, such as geometrical spreading, anelastic attenuation, and scattering, all of which are responsible for diminishing the amplitude of the waves with travel distance.

For a point source, the amplitude variation with distance, for a medium with a constant anelastic coefficient is as follows (Hutton and Boore 1987):

$$-\log A_0 = a \, \log \, (R/R_{ref}) + b(R - R_{ref}) + K_{ref} \tag{7}$$

where a represents the geometrical spreading coefficient, b is the anelastic coefficient, R is the hypocentral distance, R_{ref} is the hypocentral distance at which the magnitude formula is anchored to Richter's definition, and K_{ref} is the value of this magnitude. For example, Richter (1935) established that if the maximum measured amplitude on a seismogram is 1 mm at a reference distance of 100 km, then the value of the magnitude K_{ref} is three. The choice of a reference distance K_{ref} thus depends on the differences in attenuation over the distance range covered by the data (Hutton and Boore 1987; Alsaker et al. 1991).

The value of correction S for each station-component j is determined empirically (Joyner and Boore 1981). These corrections are constrained as to sum to zero:

$$\sum_{j=1}^{n} S_j = 0 \quad j = 1, 2 \dots n \tag{8}$$

From Eqs. (6) and (7), the Wood-Anderson amplitudes $A_{i,j}$ in mm for the horizontal station components ($j = 1, 2 \dots n$) corresponding to an earthquake ($i = 1, 2 \dots m$) are:

$$\log A_{i,j} = -a \log(R_{i,j}/R_{ref}) - b(R_{i,j} - R_{ref}) + M_{L_i} - S_j - K_{ref} \tag{9}$$

The resulting equation can now be inverted to determine the unknowns (e.g., a, b, M_{L_i} and S_j) for a certain R_{ref} and their corresponding K_{ref} (Bakun and Joyner 1984). In our case, as the R_{ref} distances considered are 17 and 40 km, the corresponding K_{ref} values are 2 and 2.445, respectively.

Taking into account the following variable changes:

$$p_{i,j} = \log \, (R_{i,j}/R_{ref}), \quad q_{i,j} = (R_{i,j} - R_{ref}), \quad y_{ij} = \log \, A_{i,j} + K_{ref} \tag{10}$$

$$y_{i,j} = -a \, p_{i,j} - b \, q_{i,j} + M_{L_i} - S_j \tag{11}$$

Equation (11) becomes in matrix form,

$$
\begin{bmatrix} y_{11} \\ y_{12} \\ \vdots \\ y_{1n} \\ y_{21} \\ y_{22} \\ \vdots \\ y_{2n} \\ \vdots \\ y_{mn} \\ 0 \end{bmatrix}_{(mn+1)\times 1}
=
\begin{bmatrix}
-p_{11} & -q_{11} & 1 & 0 & \cdots & 0 & -1 & 0 & \cdots & 0 \\
-p_{12} & -q_{12} & 1 & 0 & \cdots & 0 & 0 & -1 & \cdots & 0 \\
\vdots & \vdots & \vdots & \vdots & \cdots & \vdots & \vdots & \vdots & \cdots & \vdots \\
-p_{1n} & -q_{1n} & 1 & 0 & \cdots & 0 & 0 & 0 & \cdots & -1 \\
-p_{21} & -q_{21} & 0 & 1 & \cdots & 0 & -1 & 0 & \cdots & 0 \\
-p_{22} & -q_{22} & 0 & 1 & \cdots & 0 & 0 & -1 & \cdots & 0 \\
\vdots & \vdots & \vdots & \vdots & \cdots & \vdots & \vdots & \vdots & \cdots & \vdots \\
-p_{2n} & -q_{2n} & 0 & 1 & \cdots & 0 & 0 & 0 & \cdots & -1 \\
\vdots & \vdots & \vdots & \vdots & \cdots & \vdots & \vdots & \vdots & \cdots & \vdots \\
-p_{mn} & -q_{mn} & 0 & 0 & \cdots & 1 & 0 & 0 & \cdots & -1 \\
0 & 0 & 0 & 0 & \cdots & 0 & 1 & 1 & \cdots & 1
\end{bmatrix}_{(mn+1)\times(m+n+2)}
\times
\begin{bmatrix} a \\ b \\ M_{L_1} \\ M_{L_2} \\ \vdots \\ M_{L_m} \\ S_1 \\ S_2 \\ \vdots \\ S_n \end{bmatrix}_{(m+n+2)\times 1}
\tag{12}
$$

or simply

$$y = G\,x \tag{13}$$

is a system of $(mn) + 1$ linear equations, G is the kernel matrix of size $((m \times n) + 1) \times (m + n + 2)$, x is the parameter vector with $(m + n + 2)$ unknowns, and y is the observation vector of $(mn) + 1$ elements.

To solve Eq. (13), we need to calculate the inverse of the large matrix G. Because G is not a square matrix, we use the generalized inverse matrix (Langston et al. 1998) by applying the singular value decomposition method implemented in MATLAB. In the same way, the calculation of the variance–covariance matrix allows us to obtain the uncertainties for each of the unknowns (a, b, M_{L_i} and S_j).

Obtaining parameters a and b, and the station corrections S_j, allows us to generate the local magnitude, M_L, from the measurement of the maximum S wave amplitude, A, in mm, in the synthesized horizontal-component Wood-Anderson recordings (Kanamori and Jennings 1978; Uhrhammer and Collins 1990; Uhrhammer et al. 1996):

$$M_L = \log A + a \log \left(R/R_{ref} \right) + b \left(R - R_{ref} \right) + K_{ref} + S \tag{14}$$

A large number of earthquakes and observations increases the size of the matrices considerably so that a large calculation capacity is required for the inversion process. In our case, we had access to the Magerit Supercomputer belonging to the Universidad Politécnica de Madrid (Madrid, Spain),
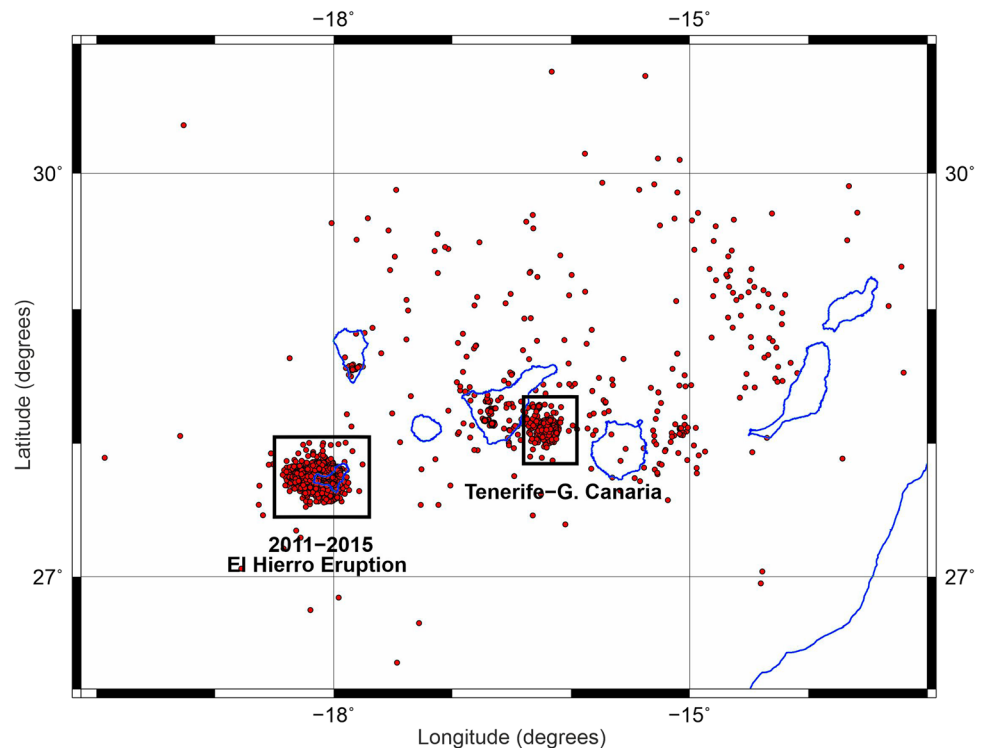
which consists of a cluster of 68 ThinkSystem SD530 nodes, each equipped with Intel Xeon Gold 6230 processors (20 cores @ 2.1 GHz), 192 GB of RAM and 480 GB SSD. This configuration is capable of providing a power peak of 182.78 TFLOPS.

Data and processing

For the period 2003–2020, we considered 14,002 earthquakes of magnitudes $m(Lg) \geq 1.5$ all of which had more than six stations covering the hypocentral location. Following Richter's (1935) methodology, we only considered the horizontal components. However, we also explored the possibility of using the vertical component because, for stations located on rocks (Havskov and Ottemöller 2010), the maximum vertical and horizontal amplitudes are similar. In our case, we found that the magnitudes from the vertical components were systematically 17% smaller than those obtained for the horizontal components, this being due to the different substrate types of the station sites. Consequently, we consider only the horizontal components. Thus, given these conditions, a total of 159,787 records were extracted from the continuous databank of the IGN.

However, during part of the period considered, an eruption and its associated seismic crisis occurred at El Hierro (López et al. 2012). Thus, we decided to separately consider the seismicity associated with the period of 2011–2015 at El Hierro so as to avoid biasing data sets with a large number

Fig. 2 Seismicity used in this paper corresponds to the 2011 El Hierro eruption and with a focus on the islands of Gran Canaria and Tenerife. The data set consists of the total seismicity for the Canary Islands with the exception of data corresponding to the 2011–2015 El Hierro eruption

Fig. 3 Map of the Canary Islands and the IGN stations used in this study

of purely volcanic event types. Moreover, we included the seismicity occurring between the islands of Tenerife and Gran Canaria in the general study and considered it separately, because, this activity is the greatest foci of supposed tectonic origin. The map giving the earthquake locations of the three data sets is shown in Fig. 2, and stations employed in the inversion process are identified in Fig. 3.

For each selected record, the complete waveform was extracted from time windows that were 300 s in length, spanning 60 s of data before any given origin time and 240 s after. The selected records were filtered with a Butterworth filter of 0.5–20 Hz with 4 poles, the DC was eliminated, and the signal was tapered with a cosine window as a prior step to deconvolution with its instrumental response to obtain the ground velocity record (GVR). The waveforms of the GVR were convolved with the Wood-Anderson (WA) response curve to obtain the waveforms recorded by this type of seismograph. The original characteristics of the WA instrument (natural period $T = 0.8$ s, damping constant $h = 0.8$ and static magnification $V = 2800$) were changed following Uhrhammer and Collins (1990) to $h = 0.7$ and $V = 2080$.

Once the GVR and WA records were obtained from the IGN databank, three-time windows were automatically selected. The first was a noise window lasting 10 s before the origin time. The second corresponded to the P wave window and had a duration of 4 s around its theoretical arrival as obtained from the velocity structure model used in the hypocentral location process. Finally, the third was the S wave, whose onset was 5 s before the theoretical S wave arrival and had a variable duration depending on the hypocentral distance (varying from 10 s for distances less than 40 km to 35 s for distances between 400 and 500 km).

The amplitude values of the S wave were automatically measured in the time window and corresponded to the zero-to-maximum signal within the window. This automatic procedure was performed with the Seismic Analysis Code (SAC) (Goldstein and Snoke 2005), and an example of the automatic S wave maximum amplitude is shown in Fig. 4. Stations with a signal-to-noise ratio for the S wave less than seven were discarded. We also eliminated all spurious amplitude spikes and peaks produced by instrumental problems or due to issues with the instrumental response. The criterion for this filtering was that if the magnitude value obtained by applying the original Richter magnitude M_L as given by Hutton and Boore (1987) differed from the catalog magnitude $m(Lg)$ by more than one magnitude unit, then the record was removed. After filtering, 93,104 WA amplitude observations corresponding to 8677 earthquakes were available for analysis. Figure 5 shows the logarithm of the final WA amplitude in mm as a function of the hypocentral distance.

Results

Attenuation across the Canary Islands

Given that the Canary Islands are tectonically complex zones with varying seismic quality factor Q-values whose seismicity extends over an oceanic and volcano island environment, a single attenuation function for the entire volcano island chain needs to be tested. For this reason, four data sets were considered:

Fig. 4 Example showing the automatic process for isolating the noise prior to the signal and the time segment in which P and S are found in the velocity record, with the maximum for the corresponding S wave for the N-S component from the TBT station on La Palma. On the right, the same segments are for the synthetic Wood-Anderson filtered data
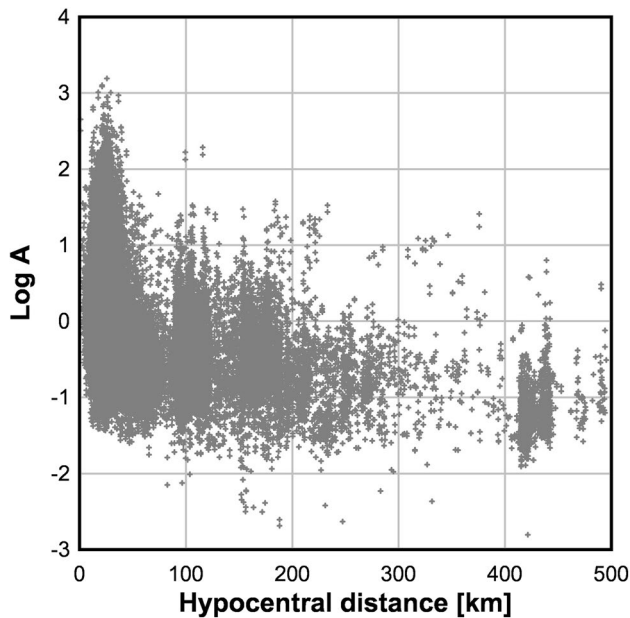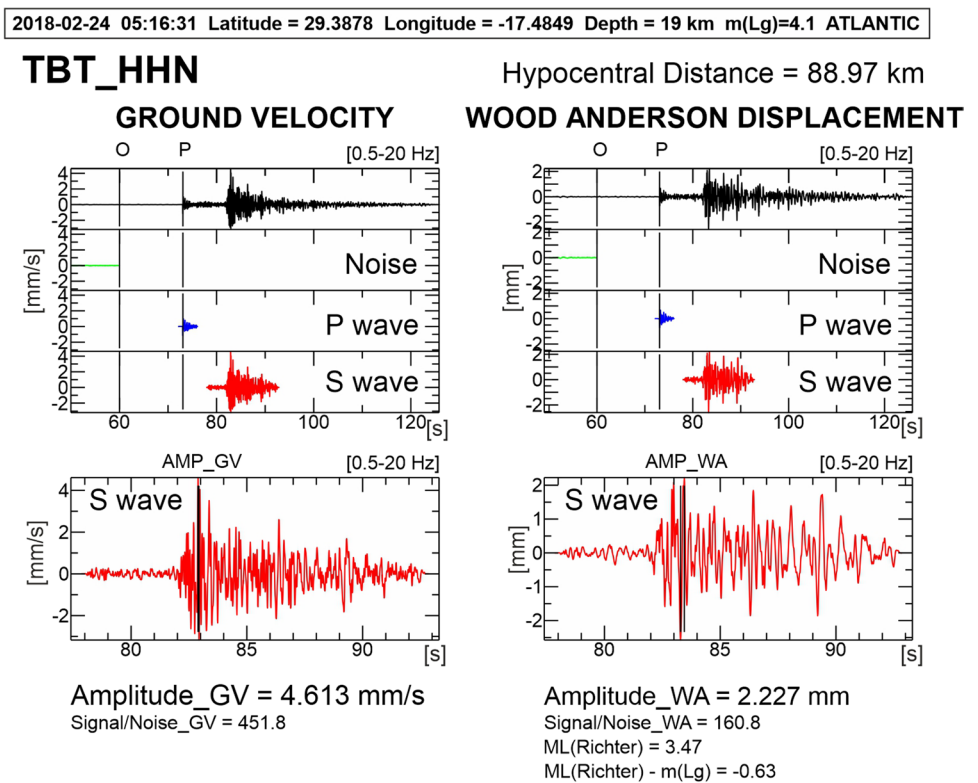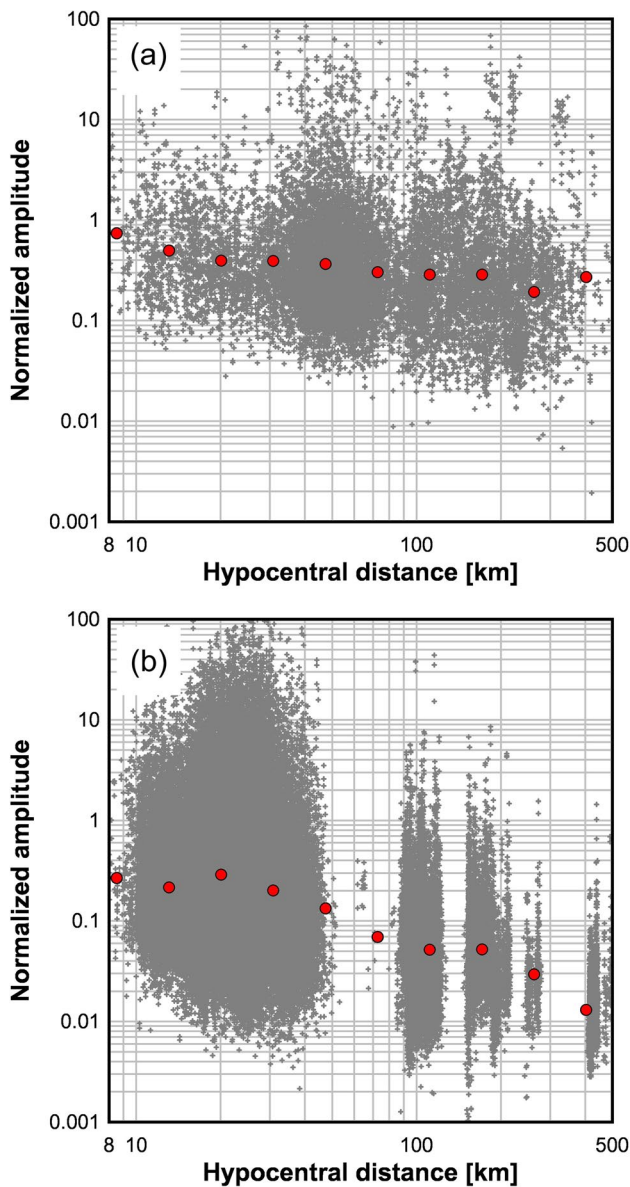

Fig. 5 Logarithm of the WA amplitudes in mm was selected as a function of the hypocentral distance in km

earthquakes and 71,194 observations from stations on the island.

(2) The second data set (data set 2) corresponds to the recurrent seismicity occurring between the islands of Gran Canaria and Tenerife (Fig. 2), which consists of 346 earthquakes and 3795 observations from the stations on these two islands.

(3) The third data set (data set 3) corresponds to all seismicity occurring in the archipelago (except from El Hierro in 2011–2015) and consists of 696 earthquakes and 9267 observations that are representative of the seismicity occurring on the Canary Islands as a whole.

(4) Finally, a data set (data set 4) of 8677 selected earthquakes and 93,104 observations was also considered, which includes the whole set of data and all recording stations.

An important question to be answered for each data set is whether just one amplitude decay with distance should be taken into account or whether bilinear or trilinear attenuation needs to be considered. For example, piecewise attenuation may occur as a consequence of postcritical Moho reflections at certain epicentral distances (Burger et al. 1987; Atkinson and Wald 2007; Atkinson et al. 2014; Mezcua et al. 2020). Figure 6a shows the normalized amplitudes for the data set from the Canary Islands, including El Hierro 2011–2015 eruption seismicity, in which the amplitude diminishes

(1) The first data set (data set 1) corresponds to the eruption on El Hierro and the associated seismicity that occurred on and around the island during the 2011–2015 crisis (Fig. 2). This data set consists of 7623

Fig. 6 **a** Decay of the normalized Wood-Anderson amplitudes in the 10–40 km distance bin as a function of the hypocentral distance (red dots) for the data set (gray crosses) corresponding to the Canary Islands (excluding data for the 2011–2015 El Hierro eruption); **b** decay of the normalized Wood-Anderson amplitudes in the 10–40 km distance bin as a function of the hypocentral distance (red dots) for data (gray crosses) from the 2011–2015 El Hierro eruption

the individual amplitudes at all distances using the geometric mean of that interval.

However, in Fig. 6b, we consider only the data corresponding to the 2011–2015 eruption on El Hierro and perform normalization of all amplitudes at a very short distance interval of 15–30 km. Here we observe an increase that is compatible with the simultaneous arrival of direct waves originating from earthquakes at a depth of 10 km, and waves refracted and reflected at Moho depths of 15–17 km with an average crustal P wave velocity of 7.4 km/s. We thus can conclude that, for the Canary Islands data set, if we exclude data from the 2011–2015 eruption on El Hierro, a linear attenuation pattern explains the observed data.

A local magnitude scale for earthquakes across the Canary Islands

By inverting Eq. (13) and using the different data sets, we can obtain different values for attenuation coefficients a and b. Table 1 shows the values for the data sets considered in the final iteration, which are given along with their respective errors. To control a possible trade-off between coefficients a and b, we add to Table 1 a constrained solution for the inversion of Eq. (13), with the condition $a = 1$ for all data sets. Data set 1 corresponds to a selection of 696 earthquakes from the Canary Islands (Fig. 2). The corresponding epicenter station paths cover most of the archipelago and surrounding regions and are shown in Fig. 7. This data set thus represents the seismicity from the entire Canary Islands chain and consists of 9627 horizontal WA amplitude observations with a geometrical spreading coefficient of 0.967 and a b-value corresponding to an intrinsic attenuation of 0.00142. Figure 8d shows that the maximum hypocentral distance distribution of the WA observations is in the 30–50 km distance range, which justifies the selection of 40 km as the reference distance (R_{ref}). In addition, due to the varying origin of the observed seismicity in the different parts of the islands, a reference distance out of the focus of the earthquake is needed. Figure 8 also depicts the annual distribution of the seismicity considered for data set 1 (Fig. 8a), together with the $m(Lg)$ values considered for this inversion (Fig. 8b) and its depth distribution (Fig. 8c). The distribution of the magnitude residuals between the final local magnitude for each event (with station corrections applied) and the individual values determined for each station and component are shown in Fig. 9. No trend with distance is observed, indicating that the residuals follow a normal distribution.

The observed anelastic coefficient b for an S wave of velocity β can be converted into the corresponding quality factor Q for a frequency f using $Q = \pi f / (\beta b \ln 10)$.

linearly with distance. Normalization eliminates differences in the source size and shows only the attenuation characteristics of the area. Given that the distances are represented on a logarithmic scale, normalization in a single distance bin of 10–40 km can be calculated using a geometric mean (Yenier 2017; Kavoura et al. 2020). In other words, for each event, we can calculate the geometric mean of the amplitudes that belong to the selected distance bin and normalize

Table 1 Values of coefficients obtained for the data sets

Dataset	a	b	σ	Rref	Kref	Evt	Obs	Distance Range [km]
Canary Islands	0.967 ± 0.019	0.00142 ± 0.00008	0.18	40	2.445	696	9267	10–500
	1 (fixed)	0.00131 ± 0.00005	0.18	40	2.445	696	9267	10–500
El Hierro eruption (2011–2015)	0.186 ± 0.007	0.01657 ± 0.00032	0.17	17	1.989	7623	71,194	5–80
	1 (fixed)	-0.01202 ± 0.00020	0.18	17	1.989	7623	71,194	5–80
	1 (fixed)	-0.00520 ± 0.00028	0.17	17	1.989	4150	38,467	20–80
Tenerife-Gran Canaria	0.389 ± 0.129	0.00915 ± 0.00127	0.15	40	2.445	346	3795	20–120
	1 (fixed)	0.00351 ± 0.00043	0.15	40	2.445	346	3795	20–120
All seismicity	0.460 ± 0.040	0.00330 ± 0.00003	0.17	40	2.445	8677	93,104	10–500
	1 (fixed)	0.00100 ± 0.00003	0.19	40	2.445	8677	93,104	10–500

Fig. 7 Ray-path surface projections between the selected earthquakes for the Canary Islands (red circles) and the stations used in this study
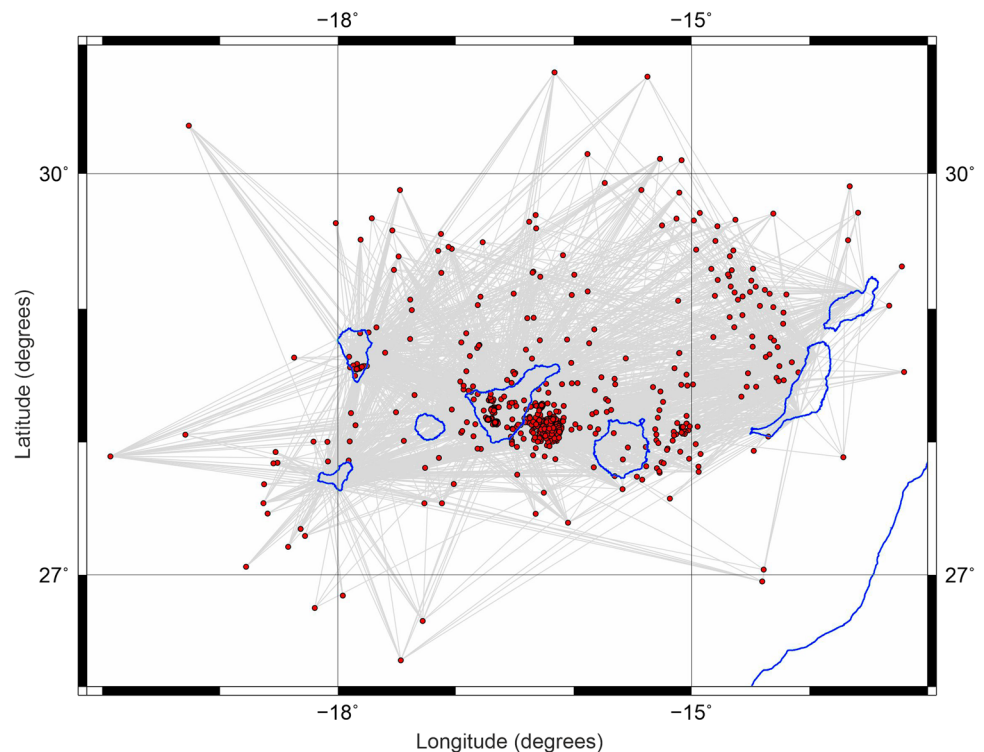
However, the resulting Q should be treated with caution for two reasons. First, there is a trade-off between the intrinsic attenuation and the geometrical spreading. Second, the considered amplitudes in the log A data do not correspond to a single seismic phase at a unique frequency (Bakun and Joyner 1984).

The second data set considered separately (data set 2, Table 1) corresponds to the eruption on El Hierro and considers the amplitudes from the stations on El Hierro. The corresponding values for geometrical spreading ($a = 0.186$) and intrinsic attenuation ($b = 0.01657$) are quite different from data set 1, as is to be expected in the case of comparing events associated with a volcanic eruption with the general volcano-tectonic events for the chain as a whole. In the case of data set 2, the selected reference distance was 17 km. This shorter distance was used because: (1) our aim was to use the focus of the activity as a reference value, and (2) the maximum of the hypocentral distance distribution lies within this distance range. Two solutions for the condition $a = 1$ were obtained for the distance intervals of 5–80 and 20–80 km (Table 1). The solutions obtained for b are -0.01202 and -0.00520 for the two distance intervals, respectively. As we discuss below, this, physically, makes no sense.

Finally, we considered the data sets corresponding to the seismicity occurring between the islands of Tenerife and

Fig. 8 Histograms showing different aspects of the data: **a** distribution of the yearly number of earthquakes. The sudden increase after 2017 corresponds to a notable increase in the number of stations; **b** distribution of the levels of magnitude; **c** distribution of the depth of the earthquakes; **d** distribution of the hypocentral distances from stations. The greatest frequency of distances corresponds to the 40 km hypocentral distance
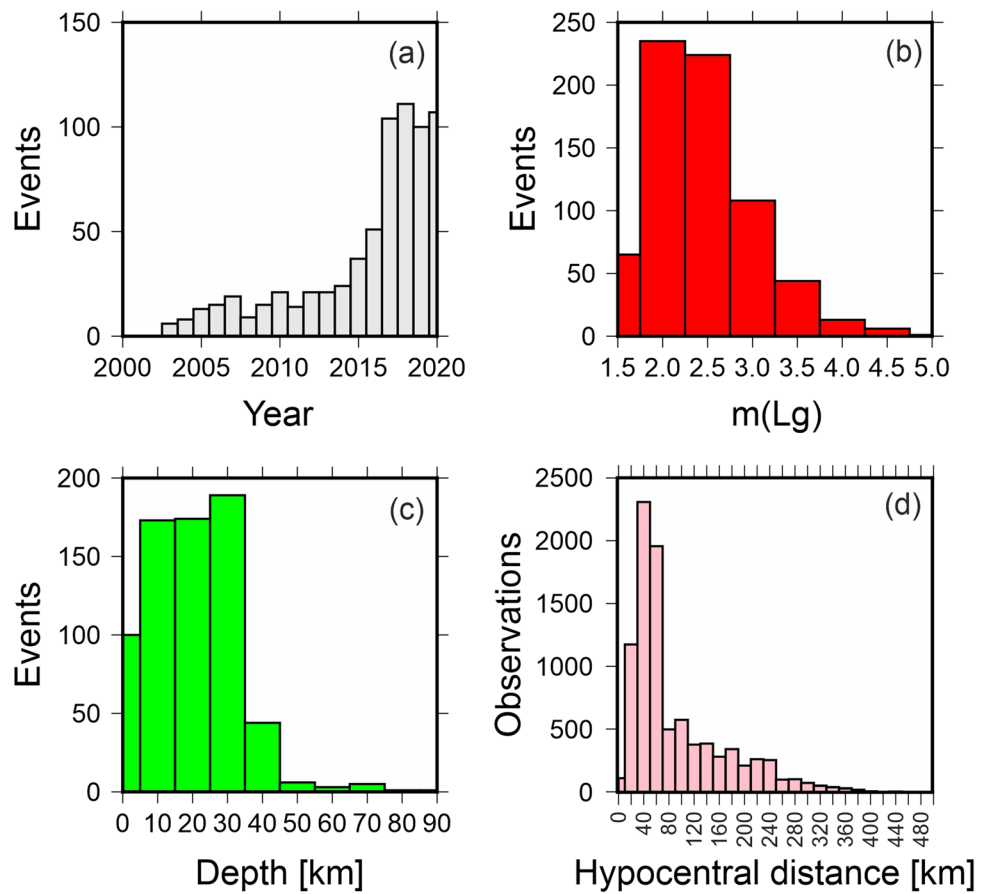

Fig. 9 Local magnitude residuals (station and component values minus the average event magnitude) as a function of hypocentral distance and histogram of the residuals
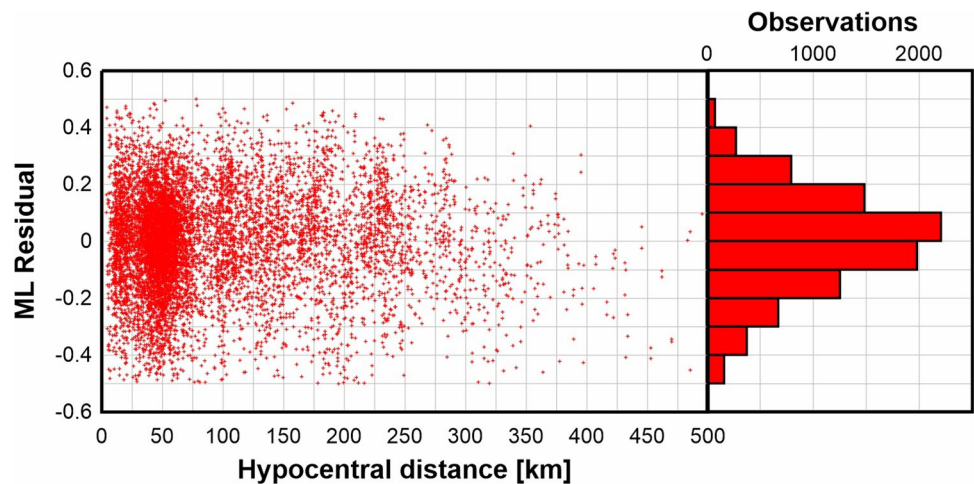
Gran Canaria (data set 3, Table 1), which is by no means the most frequent focus of seismicity in the archipelago, and the data corresponding to the total seismicity for the whole archipelago (data set 4, Table 1). The derived a and b values for data set 3 are 0.389 and 0.00915, respectively. Note that this solution is obtained using data only from stations on Tenerife and Gran Canaria. In this case, the constrained inversion with $a = 1$ and the corresponding $b = 0.00351$ is

our preferred solution (Table 1). Finally, if we consider the total seismicity data set (data set 4), the b-values obtained for the constrained inversion are also our preferred solution ($a = 1$, $b = 0.00100$).

The corresponding $-\log A_0$ values for the four data sets can be compared with the values of $-\log A_0$ derived by Hutton and Boore (1987) for California and López (2008) for the Iberian Peninsula (Fig. 10a). At a glance, we can
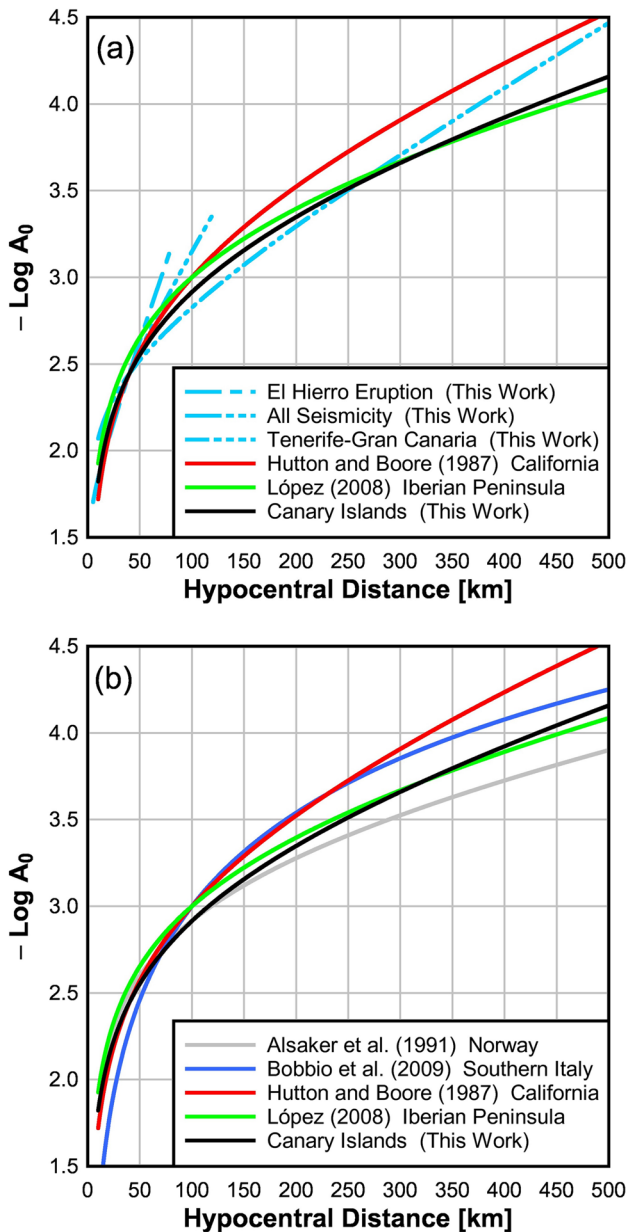
Fig. 10 **a** Comparison of attenuation curves obtained in this work for the data from the eruption on El Hierro, all the seismicity selected for the study area, the Tenerife-Gran Canaria data set and the data corresponding to the whole Canary Archipelago, as well as the attenuation curves for California (Hutton and Boore 1987) and the Iberian Peninsula López (2008). **b** Comparison of the representative attenuations obtained for the Canary Islands and for Norway (Alsaker et al. 1991), southern Italy (Bobbio et al. 2009), California (Hutton and Boore 1987), and the Iberian Peninsula (López 2008)

Fig. 11 Correlation of local magnitudes obtained in this work with the corresponding m(Lg) from López (2008) given in the official seismic catalog. The discontinuous line represents the ± 1 standard deviation

observe that the Hutton and Boore (1987) derivation produces greater $-\log A_0$ values over the 50–500 km distance interval, which implies greater attenuation in the Canary Islands data set. However, for a smaller distance range, the opposite occurs. Instead, values obtained using the López (2008) derivation show greater attenuation up to a distance of 350 km, from which point the tendency is inverted. In a general sense, the Hutton and Boore (1987) and López (2008) $-\log A_0$ values are greater than the values derived here for the Canary Islands. This is because they represent attenuation through continental crustal structures, while the attenuation for the Canary Islands passes through oceanic structures. The attenuation curves representing the other three data sets considered for the Canary Islands show similar tendencies to those described above, albeit over more limited distance ranges.

It is not possible to compare the attenuation correction for the Canary Islands with the corresponding m(Lg) because the latter is not a local magnitude. We thus performed a correlation between the M_L and m(Lg) values for the same earthquakes provided by these different definitions (Fig. 11). The general trend shows that, above an M_L magnitude of three, our M_L values are lower than the corresponding m(Lg). The derived relationship is thus:

$$m(\text{Lg}) = 0.618 + 0.867\,M_L \tag{15}$$

with a correlation coefficient (R^2) of 0.87.

Table 2 List of corrections in the horizontal components for the 37 broadband stations and the different data sets

| STA	Vs30 [m/s]	All seismicity		Canary Islands		Tenerife-Gran Canaria		El Hierro eruption (2011–2015)	
		HHE	HHN	HHE	HHN	HHE	HHN	HHE	HHN
CADE	918	0.37 ± 0.03	0.30 ± 0.03	0.34 ± 0.03	0.27 ± 0.03	0.32 ± 0.08	0.28 ± 0.06		
CBLA		− 0.04 ± 0.04	− 0.14 ± 0.04	0.04 ± 0.04	0.03 ± 0.05				
CBOL		0.25 ± 0.01	0.25 ± 0.01	0.11 ± 0.02	0.11 ± 0.02	− 0.06 ± 0.02	− 0.10 ± 0.02		
CBRE		− 0.17 ± 0.02	− 0.19 ± 0.02	− 0.23 ± 0.03	− 0.23 ± 0.03				
CCAL		− 0.37 ± 0.02	− 0.40 ± 0.02	− 0.21 ± 0.04	− 0.28 ± 0.04				
CCAN		0.47 ± 0.01	0.51 ± 0.01	0.38 ± 0.01	0.42 ± 0.02	0.26 ± 0.01	0.30 ± 0.02		
CDOS		0.08 ± 0.02	0.10 ± 0.02	− 0.02 ± 0.02	0.02 ± 0.02	− 0.10 ± 0.02	− 0.07 ± 0.03		
CENR		− 0.19 ± 0.02	− 0.14 ± 0.02	− 0.28 ± 0.03	− 0.19 ± 0.03				
CFLP		− 0.18 ± 0.04	− 0.26 ± 0.04	− 0.20 ± 0.06	− 0.29 ± 0.05				
CFTV		0.31 ± 0.02	0.24 ± 0.02	0.34 ± 0.02	0.25 ± 0.02				
CFUE		− 0.01 ± 0.01	− 0.06 ± 0.01	0.13 ± 0.01	0.10 ± 0.01				
CGIN		0.25 ± 0.02	0.25 ± 0.02	0.26 ± 0.02	0.25 ± 0.02				
CGOR		0.11 ± 0.03	0.17 ± 0.04	0.08 ± 0.05	0.02 ± 0.05				
CGRA	512	0.05 ± 0.02	0.08 ± 0.02	− 0.01 ± 0.02	0.00 ± 0.02	− 0.13 ± 0.02	− 0.11 ± 0.02		
CGUI	535	− 0.05 ± 0.01	− 0.06 ± 0.01	− 0.13 ± 0.01	− 0.13 ± 0.01	− 0.21 ± 0.01	− 0.22 ± 0.01		
CJED		− 0.20 ± 0.03	− 0.16 ± 0.03	− 0.16 ± 0.04	− 0.18 ± 0.04				
CLLA		− 0.04 ± 0.04	− 0.12 ± 0.04	− 0.18 ± 0.05	− 0.20 ± 0.05				
CLUM		0.24 ± 0.02	0.15 ± 0.02	0.12 ± 0.02	0.06 ± 0.02				
CMIR		0.01 ± 0.02	0.03 ± 0.02	0.00 ± 0.02	− 0.02 ± 0.02				
CNAO		− 0.39 ± 0.02	− 0.31 ± 0.02	− 0.16 ± 0.04	− 0.17 ± 0.04				
CPUN		− 0.05 ± 0.03	− 0.05 ± 0.03	− 0.09 ± 0.03	− 0.14 ± 0.04				
CRAJ		− 0.17 ± 0.01	0.08 ± 0.01	− 0.30 ± 0.01	− 0.04 ± 0.01	− 0.41 ± 0.01	− 0.14 ± 0.01		
CREA	482	− 0.02 ± 0.01	− 0.02 ± 0.01	− 0.12 ± 0.01	− 0.12 ± 0.01	− 0.23 ± 0.02	− 0.24 ± 0.02		
CROM		0.07 ± 0.04	− 0.02 ± 0.04	− 0.16 ± 0.06	− 0.18 ± 0.05				
CTAC	326	− 0.24 ± 0.02	− 0.23 ± 0.02	− 0.11 ± 0.05	− 0.29 ± 0.05				
CTEN		− 0.24 ± 0.03	− 0.19 ± 0.03	− 0.29 ± 0.05	− 0.23 ± 0.04				
CTFS		0.13 ± 0.01	0.23 ± 0.02	0.05 ± 0.02	0.17 ± 0.02	− 0.01 ± 0.02	0.09 ± 0.02		
CTIG	408	0.13 ± 0.01	0.21 ± 0.01	0.15 ± 0.03	0.24 ± 0.03			0.54 ± 0.01	0.62 ± 0.01
CVIL		0.14 ± 0.06	0.15 ± 0.05	0.10 ± 0.06	0.18 ± 0.05	0.01 ± 0.05	0.03 ± 0.05		
EBAJ		0.51 ± 0.01	0.60 ± 0.01	0.41 ± 0.01	0.40 ± 0.01	0.37 ± 0.01	0.34 ± 0.01		
EFAM		0.40 ± 0.02	0.41 ± 0.02	0.54 ± 0.03	0.54 ± 0.03				
EGOM		0.23 ± 0.01	0.22 ± 0.01	0.04 ± 0.01	0.02 ± 0.01				
EHIG		0.13 ± 0.01	0.13 ± 0.01	0.05 ± 0.03	0.02 ± 0.03				
EOSO		0.57 ± 0.01	0.51 ± 0.01	0.33 ± 0.02	0.30 ± 0.01	0.25 ± 0.02	0.21 ± 0.02		
GGC		0.13 ± 0.02	0.17 ± 0.02	0.05 ± 0.02	0.08 ± 0.02	− 0.01 ± 0.02	0.01 ± 0.02		
MACI		0.44 ± 0.01	0.43 ± 0.01	0.26 ± 0.01	0.26 ± 0.01	0.18 ± 0.02	0.18 ± 0.02		
TBT		0.43 ± 0.02	0.43 ± 0.02	0.40 ± 0.03	0.41 ± 0.03				

Station correction terms

The four data sets were used to generate station corrections (STA_CORR) for 106 horizontal components for the 37 broadband stations shown in Table 2 and the 16 short-period stations in Table 3. We have also added to Tables 2 and 3 the average shear velocity down to a depth of 30 km (Vs30) determined for some of the same stations by Núñez (2017). According to Eq. (6), a positive value for a station correction implies that the corrected magnitude value for such a station will increase over the uncorrected M_L, and the opposite will be true for negative values. These corrections are associated mainly with the influence of station site effects so that the correction takes into account the intrinsic relationship for the type of ground on which the station is installed. We find that, the station corrections for the same station location using different data sets or different instruments have the same sign (positive or negative) and almost the same value.

Table 3 List of corrections in the horizontal components for the 16 short-period stations and the different data sets

STA	Vs30 [m/s]	All seismicity		Canary Islands		Tenerife-Gran Canaria		El Hierro eruption (2011–2015)	
		EHE	EHN	EHE	EHN	EHE	EHN	EHE	EHN
CADE	918	0.40 ± 0.04	0.44 ± 0.04	0.31 ± 0.04	0.39 ± 0.05	0.26 ± 0.05	0.37 ± 0.06		
CCAL			-0.38 ± 0.13						
CCHO		0.09 ± 0.02	0.19 ± 0.02	0.01 ± 0.02	0.12 ± 0.02	-0.11 ± 0.02	-0.03 ± 0.02		
CCUM	321	-0.32 ± 0.01	-0.16 ± 0.01	-0.18 ± 0.03	-0.01 ± 0.03			0.54 ± 0.01	0.62 ± 0.01
CFOR		-0.01 ± 0.02	-0.02 ± 0.02	-0.11 ± 0.02	-0.13 ± 0.02	-0.19 ± 0.02	-0.20 ± 0.02		
CJUL	300	-1.53 ± 0.01	-1.57 ± 0.01	-0.46 ± 0.03	-0.45 ± 0.04			0.13 ± 0.01	0.29 ± 0.01
CNAO	389	-0.33 ± 0.08	-0.23 ± 0.08						
CNOR		-0.21 ± 0.01	-0.19 ± 0.01	-0.30 ± 0.01	-0.28 ± 0.01	-0.41 ± 0.01	-0.39 ± 0.01	-1.09 ± 0.01	-1.13 ± 0.01
CORC		-0.38 ± 0.01	-0.47 ± 0.01	-0.27 ± 0.04	-0.32 ± 0.04				
CROM		-0.06 ± 0.04	-0.09 ± 0.04	-0.21 ± 0.05	-0.22 ± 0.05				
CRST	389	-0.45 ± 0.01	-0.38 ± 0.01	-0.12 ± 0.04	-0.08 ± 0.04			0.09 ± 0.01	0.01 ± 0.01
CTAB	308	-0.43 ± 0.01	-0.38 ± 0.01	-0.18 ± 0.03	-0.16 ± 0.03				
CTAN	350	-0.31 ± 0.01	-0.22 ± 0.01	-0.28 ± 0.02	-0.15 ± 0.03			-0.01 ± 0.01	0.06 ± 0.01
CVIE		-0.04 ± 0.05	-0.21 ± 0.04	-0.16 ± 0.07	-0.22 ± 0.07				
CVIL		0.29 ± 0.03	0.29 ± 0.03	0.21 ± 0.03	0.20 ± 0.03	0.13 ± 0.03	0.15 ± 0.03		
GUIA		0.10 ± 0.02	0.17 ± 0.02	0.02 ± 0.02	0.10 ± 0.02	-0.13 ± 0.02	-0.07 ± 0.02		
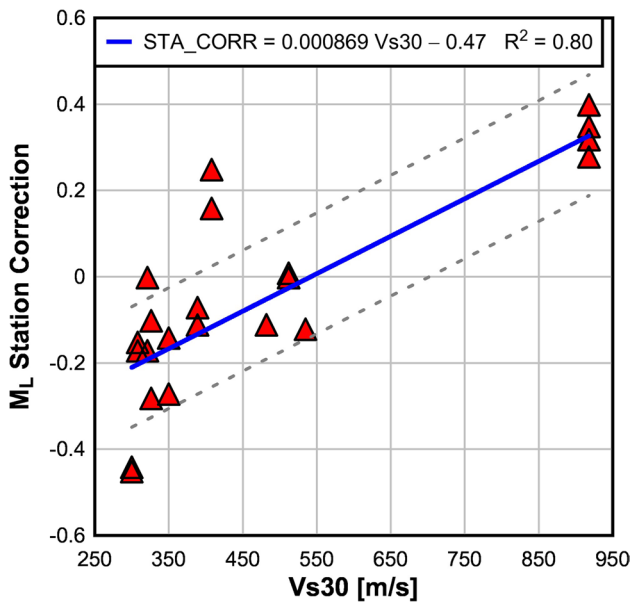
Fig. 12 Station correction compared to their respective Vs30 values for stations with this information. The discontinuous line represents ± 1 standard deviation

Figure 12 shows a linear correlation between the derived station corrections and the Vs30 values given in Núñez (2017). Using this correlation, it is possible to obtain an approximation for the station correction value for any new stations by determining Vs30 and using the following relationship (Fig. 12):

$$STA\_CORR = 0.000869 \, Vs30 - 0.47 \quad (16)$$

with a (R^2) correlation coefficient of 0.80.

Discussion

So as to consider a large amount of data for earthquakes spanning an entire volcano island chain, we specifically designed a procedure to search for the selected data in the database (amplitudes and hypocentral distances) and convert it to Wood-Anderson amplitudes. These amplitudes were then inverted so as to obtain the local magnitude parameters. Because our approach may serve as a blueprint and benchmark for setting M_L scales at other volcanically active regions, details of this procedure have been fully described in the Data and Processing above, and the results are given in Tables 1, 2, and 3.

Our analysis of the general trend of the Wood-Anderson amplitudes for the four different data sets (with the exception of those corresponding to the eruption on El Hierro, e.g., data set 2) shows an attenuating linear trend for the hypocentral distance. This result enables us to consider a single linear attenuation expression for the whole region (Fig. 6). However, the data from the eruption on El Hierro show an increase in amplitude in the 10–25 km distance range that can be interpreted by the simultaneous arrival at the surface of direct, refracted, and reflected S waves at the Moho surface from the waves originating at a depth

of 10 km. This interpretation is compatible with the non-sensical b-values of -0.01202 and -0.00520 obtained for the constrained solution (e.g., $a = 1$) for the two different distance intervals. These parameters reflect an anomalous amplitude increase with distance. No attempt was made to take into account trilinear attenuation for these data because it was not used in the Canary Islands data set.

The trade-off between geometrical spreading and intrinsic attenuation implies that our interpretation of the parameters that represent the intrinsic attenuation in terms of the internal friction Q^{-1} of the medium is restricted to the local case considered. The obtained local magnitude formula for the Canary Islands (the Canary Islands data set) for a reference distance R_{ref} of 40 km is

$$M_L = \log A + 0.967 \log (R/40) + 0.00142 (R - 40) + 2.445 + S \tag{17}$$

Here A is the maximum amplitude of the S wave in mm in the synthetic Wood-Anderson record, R is the hypocentral distance in km, and S is the correction for the corresponding station component as given in Tables 2 and 3.

The attenuation for the other considered data sets is shown in Fig. 10a, along with a comparison with the corresponding $-\log A_0$ calculated by Hutton and Boore (1987) for California (horizontal strike-slip motion between two plates) and López (2008) for Iberia (convergent plate boundary) and those obtained in this paper (hot spot island chain on an oceanic crust). In terms of the data for Tenerife and Gran Canaria, the $-\log A_0$ between these two volcanic islands within the ancient Jurassic oceanic crust (Hayes and Rabinowitz 1975) corresponds to the constrained solution with an anelastic coefficient value compatible with a brittle material and of the same order than the found for the East African Plateau formed by several Precambrian terranes (Langston et al. 1998). Mezcua and Rueda (2021) reached a similar conclusion interpreting that the low slope parameter (0.5) of the Gutenberg–Richter recurrence law obtained for the seismicity in this specific area is also compatible with a brittle material and highly effective stress (Mogi 1962; Wyss et al. 2001).

For comparison, in Fig. 10b, we show the $-\log A_0$ obtained for our Canary Islands, along with a selection of $-\log A_0$ values from other parts of the world. The nearest relationship corresponds to the calculation by López (2008) for the Iberian Peninsula. At distances up to 325 km, our relationship provides smaller magnitudes, reaching 0.05 units at 150 km. However, if we compare our calculations with Norway (Alsaker et al. 1991), for instance, our relationship gives similar magnitudes at distances out to 100 km. However, for greater distances, our relation gives greater magnitudes, reaching 0.15 units at 300 km. Finally, the comparison with southern Italy (Bobbio et al. 2009) indicates that out to 70 km, our relationship gives greater magnitudes

(by an order of 0.15 units). However, at 300 km, our magnitudes are 0.20 units lower than those obtained using the M_L system of Bobbio et al. (2009).

The M_L station corrections derived here for our Canary Islands data set apply to 51 stations (102 horizontal components) and lie in a STA_CORR limited range of $[-0.54, +0.54]$. This correction shows a correlation with the substrate characteristics of each station site as characterized by Vs30. The correction values for all stations when data sets 1, 3, and 4 coincide. However, the exception is the data for the stations on El Hierro that recorded events during the 2011 eruption. These events were biased by great volcanic tremors.

Conclusions

We here derive for the first time an M_L scale for the Canary Islands-based on data from 696 earthquakes and 9267 horizontal WA synthetic observations recorded by 51 broadband and short-band stations. The catalog used considers all earthquakes between 1.5 and 4.9 m(Lg) recorded for the Canary Islands during the period of 2003–2020. We find that the distance correction term for the Canary Islands is greater than that calculated by Hutton and Boore (1987) for California and by López (2008) for the Iberian Peninsula, although in the latter case, the term operates only in a distance range of 0–325 km. The attenuation pattern was linear throughout the island chain except during the El Hierro eruption when the amplitude decay displayed a trilinear decay with an increase in the 10–25 km distance range. We interpret this as having been caused by the simultaneous arrival of direct waves from earthquakes at a depth of 10 km with refracted and reflected waves at Moho depths of 15–17 km. However, any attempt to associate a physical significance to the parameters of geometrical spreading and intrinsic attenuation is hampered by the long distances of the paths (0–500 km) involved and the fact that geometrical spreading is influenced by the distance traveled (Di Bona 2016).

The station corrections derived from the inversion process are restricted to the $[-0.54, +0.54]$ interval and show a clear relationship with the type of ground found beneath the stations. For stations with Vs30 values, this relationship is fully satisfied, even when different data sets are used in the inversion. The use of these corrections will improve magnitude estimations for, above all, smaller earthquakes when stations have predominantly high or low Vs30 values. If uncorrected, this can result in under or overestimations of local magnitudes by up to 0.5.

The M_L definition for the Canary Islands presented here provides a more accurate determination of the magnitude of earthquakes because it considers both regional attenuations and applies site-specific corrections tailored to individual

seismic stations. The value of the presented magnitude scale was highlighted by the need for a uniform real-time response to the recent September 19, 2021 Cumbre Vieja eruption in La Palma, Canary Islands. We show here that magnitude scales for ocean island volcanoes need to be set according to local attenuation conditions. Otherwise, if generic scales derived for different tectonic settings and/or non-volcanic regions are applied, under or overestimations of the true magnitude will occur. However, we here detail a methodology that allows such a local magnitude scale to be derived, which we benchmark using nearly two decades of volcano-tectonic earthquake activity at the Canary Islands.

References

Alsaker A, Kvamme LB, Hansen RA, Dahle A, Bungum H (1991) The ML scale in Norway. Bull Seismol Soc Am 81:379–398

Anguita F, Hernán F (1975) A propagating fracture model versus a hotspot origin for the Canary Islands. Earth Planet Sci Lett 27:11–19. https://doi.org/10.1016/0012-821X(75)90155-7

Atkinson GM, Wald DJ (2007) "Did you feel it?" intensity data: a surprisingly good measure of earthquake ground motion. Seismol Res Lett 78:362–368. https://doi.org/10.1785/gssrl.78.3.362

Atkinson G, Worden CB, Wald DJ (2014) Intensity prediction equations for North America. Bull Seismol Soc Am 104:3084–3093. https://doi.org/10.1785/0120140178

Bakun WH, Joyner WB (1984) The ML scale in central California. Bull Seismol Soc Am 74:1827–1843

Banda E, Dañobeitia JJ, Surinach E, Ansorge J (1981) Features of crustal structure under the Canary Islands. Earth Planet Sci Lett 55:11–24

Bobbio A, Vassallo M, Festa G (2009) A local magnitude scale for southern Italy. Bull Seismol Soc Am 99:2461–2470. https://doi.org/10.1785/0120080364

Boore DM (1989) The Richter scale: its development and use for determining earthquake source parameters. Tectonophysics 166:1–14. https://doi.org/10.1016/0040-1951(89)90200-X

Burger R, Somerville P, Barker J, Herrmann R, Helmberger D (1987) The effect of crustal structure on strong ground motion attenuation relations in eastern North America. Bull Seismol Soc Am 77:420–439. https://doi.org/10.1785/BSSA0770020420

Canas JA, Pujades LG, Blanco MJ, Soler V, Carracedo JC (1995) Coda-Q distribution in the Canary Islands. Tectonophysics 246:245–261. https://doi.org/10.1016/0040-1951(94)00258-B

Canas JA, Ugalde A, Pujades LG, Carracedo JC, Soler V, Blanco MJ (1998) Intrinsic and scattering seismic wave attenuation in the Canary Islands. J Geophys Res 103:15037–15050. https://doi.org/10.1029/98JB00769

Carbó A, Muñoz-Martín A, Llanes P, Alvarez J, EEZ Working Group (2003) Gravity analysis offshore Canary Islands from a systematic surveying. Mar Geophys Res 24:113–127. https://doi.org/10.1007/1-4020-4352-X_5

Carracedo JC (1984) Marco Geográfico. En: Geografía Física de Canarias, vol. 1. Editorial Interinsular Canaria, Santa Cruz de Tenerife 10–16. (in Spanish)

Carracedo J, Troll V (2016) The geology of the Canary Islands. Elsevier, Amsterdam

Carracedo JC, Day SJ, Guillou H, Rodríguez Badiola E, Canas JA, Pérez Torrado FJ (1998) Hotspot volcanism close to a passive continental margin: the Canary Islands. Geol Mag 135:591–604. https://doi.org/10.1017/S0016756898001447

Condori C, Tavera H, Sant'Anna Marotta G, Peres Rocha M, Sand França G (2017) Calibration of the local magnitude scale (ML) for Peru. J Seism 21:987–999. https://doi.org/10.1007/s10950-017-9647-3

D'amico S, Maiolino V (2005) Local magnitude estimate at Mt. Etna. Ann Geophys 48:215–229. https://doi.org/10.4401/ag-3197

Dañobeitia JJ (1988) Reconocimiento geofísico de estructuras submarinas situadas al norte y sur del Archipielago Cánario. Rev Soc Geol Esp 1:143–155. (in Spanish)

Dañobeitia JJ, Canales JP (2000) Magmatic underplating in the Canary Achipelago. J Volc Geotherm Res 103:27–41. https://doi.org/10.1016/S0377-0273(00)00214-6

De la Cruz-Reyna S, Tilling R (2008) Scientific and public responses to the ongoing volcanic crisis at Popocatépetl Volcano, Mexico: importance of an effective hazards-warning system. J Volc Geotherm Res 170:121–134. https://doi.org/10.1016/j.jvolgeores.2007.09.002

del Fresno C (2016) Determinación de la fuente sísmica a distancias regionales: aplicación a la serie de El Hierro 2011. Tesis doctoral, Universidad Complutense de Madrid, Facultad de Ciencias Físicas, 228 pp + 8 anex. (in Spanish)

Del Pezzo E, Petrosino S (2001) A local-magnitude scale for Mt. Vesuvius from synthetic Wood-Anderson seismograms. J Seism 5:207–215. https://doi.org/10.1785/0120030075

Di Bona M (2016) A local magnitude scale for crustal earthquakes in Italy. Bull Seismol Soc Am 106:242–258. https://doi.org/10.1785/0120150155

Domínguez Cerdeña I, del Fresno C, Rivera L (2011) New insight on the increasing seismicity during Tenerife's 2004 volcanic reactivation. J Volc Geotherm Res 206:15–29. https://doi.org/10.1016/j.jvolgeores.2011.06.005

Dziewonski AM, Chou TA, Woodhouse JH (1981) Determination of earthquake source parameters from waveform data for studies of global and regional seismicity. J Geophys Res 86:2825–2852. https://doi.org/10.1029/JB086iB04p02825

Ekström G, Nettles M, Dziewonski AM (2012) The global CMT project 2004–2010: centroid-moment tensors for 13,017 earthquakes. Phys Earth Planet Inter 200–201:1–9. https://doi.org/10.1016/j.pepi.2012.04.002

Emery KO, Uchupi E (1984) The geology of the Atlantic Ocean. Springer Verlag, New York, p 1050

Fúster JM (1975) Las Islas Canarias: un ejemplo de evolución temporal y espacial del vulcanismo oceánico. Estudios Geol 31:439–463. (in Spanish)

García-Yeguas A, Koulakov I, Ibáñez J, Rietbrock A (2012) High resolution 3D P wave velocity structure beneath Tenerife Island (Canary Islands, Spain). J Geophys Res 117.https://doi.org/10.1029/2011JB008970

Goldstein P, Snoke A (2005) SAC Availability for the IRIS Community. Incorporated Institutions for Seismology Data Management Center Electronic Newsletter

Havskov J, Ottemöller L (2010) Routine data processing in earthquake seismology. Springer, Dordrecht, p p347

Hayes DE, Rabinowitz PD (1975) Mesozoic magnetic lineations and the magnetic Quiet Zone off Northwest Africa. Earth Planet Sci Lett 28:105–115. https://doi.org/10.1016/0012-821X(75)90217-4

Hutton LK, Boore DM (1987) The M_L scale in southern California. Bull Seismol Soc Am 77:2074–2094. https://doi.org/10.1785/BSSA0770062074

IGN (2021) IGN Catalog Spanish Digital Seismic Network. International Federation of Digital Seismograph Networks. Dataset/Seismic Network https://www.ign.es/web/ign/portal/sis-catalogo-terremotos. Last access January 2021. https://doi.org/10.7914/SN/ES

Joyner WB, Boore DM (1981) Peak horizontal acceleration and velocity from strong-motion records including records from the 1979 imperial valley, California, earthquake. Bulletin of the Seismological Society of America 71(6):2011–2038. https://doi.org/10.1785/BSSA0710062011

Kanamori H, Jennings PC (1978) Determination of local magnitude, ML, from strong-motion accelerograms. Bull Seism Soc Am 68:471–485

Kavoura F, Savvaidis A, Rathje E (2020) Determination of local magnitude for earthquakes recorded from the Texas Seismological Network (TexNet). Seismol Res Lett 91:3223–3235. https://doi.org/10.1785/0220190366

Kiliç T, Ottemöller L, Havskov J, Yanik K, Kiliçarslan Ö, Alver F, Özyazicioglu M (2017) Local magnitude scale for earthquakes in Turkey. J Seismol 21:35–46. https://doi.org/10.1007/s10950-016-9581-9

Langston CA, Brazier R, Nyblade AA, Owens TJ (1998) Local magnitude scale and seismicity rate for Tanzania, East Africa. Bull Seismol Soc Am 88:712–721

Lee WHK, Bennet RE, Meagher KL (1972) A method of estimating magnitude of local earthquakes from signal duration. US Geological Survey Open File Report 28 pp

Lodge A, Nippress SEJ, Rietbrock A, García-Yeguas A, Ibáñez J (2012) Evidence for magmatic underplating and partial melt beneath the Canary Islands derived using teleseismic receiver functions. Phys Earth Planet Int 212–213:44–54. https://doi.org/10.1016/j.pepi.2012.09.004

López C (2008) Nuevas fórmulas de magnitud para la Península Ibérica y su entorno. Trabajo de Investigación del Máster de Geofísica y Meteorología. Universidad Complutense de Madrid. Facultad de Ciencias Físicas 38 pp. (in Spanish)

López C, Blanco MJ, Abella R, Brenes B, Cabrera VM, Casas B, Domínguez-Cerdeña I, Felpeto A, Fernández de Villalta M, del Fresno C, García-Arias MJ, García-Cañada L, Gomis A, González-Alonso E, Guzmán J, Iribarren I, López-Díaz R, Luengo N, Meletlidis S, Moreno M, Moure D, Pereda J, Rodero C, Romero E, Sainz-Maza S, Sentre MA, Torres P, Trigo P, Villasante V (2012) Monitoring the volcanic unrest of El Hierro (Canary Islands) before the onset of the 2011-2012 submarine eruption. Geophys Res Lett 39. https://doi.org/10.1029/2012GL051846

López C, Benito-Saz MA, Martí J, del Fresno C, García-Cañada L, Albert H, Lamolda H (2017) Driving magma to the surface: the 2011–2012 El Hierro volcanic eruption. Geochem Geophys Geosyst 18:3165–3184. https://doi.org/10.1002/2017GC007023

Martinez-Arevalo C, Mancilla FL, Helffrich G, Garcia A (2013) Seismic evidence of a regional sublithospheric low velocity layer beneath the Canary Islands. Tectonophysics 608:586–599. https://doi.org/10.1016/j.tecto.2013.08.021

Mezcua J, Rueda J (2021) A seismicity revision and a probabilistic seismic hazard assessment using the Monte Carlo approach for the Canary Islands (Spain). Nat Hazards 108:1609–1628. https://doi.org/10.1007/s11069-021-04747-0

Mezcua J, Martínez Solares JM (1983) Sismicidad del Área Iberomogrebí. Instituto Geográfico Nacional Publicación 202 299 pp. (in Spanish)

Mezcua J, Galán J, Rueda J, Martínez Solares JM, Buforn E (1990) Sismotectónica de las Islas Canarias. Estudio del terremoto e 9 de mayo de 1989 y su serie de réplicas. Instituto Geográfico Nacional 24 pp. (in Spanish)

Mezcua J, Buforn E, Udías A, Rueda J (1992) Seismotectonics of the Canary Islands. Tectonophysics 208:447–452. https://doi.org/10.1016/0040-1951(92)90440-H

Mezcua J, Rueda J, García Blanco RM (2020) Characteristics of a new regional seismic-intensity prediction equation for Spain. Nat Hazards 101:817–832. https://doi.org/10.1007/s11069-020-03897-x

Mogi K (1962) Magnitude-frequency relation for elastic shocks accompanying fractures of various materials and some related problems in earthquakes. Bull Earthq Res Inst Tokyo Univ 40:831–853

Muñoz Lopez C, Velasquez L, Dionicio V (2020) Calibrationof Local Magnitude Scale for Colombia. Bull Seism Soc Am 110:1971–1981. https://doi.org/10.1785/0120190226

Núñez A (2017) Simulación de escenarios sísmicos mediante un sistema de información geográfica para la Península Ibérica, las Islas Baleares y las Islas Canarias, considerando el efecto de sitio y las dimensiones y características de la fuente sísmica. PhD Thesis Universidad Politécnica de Madrid. https://doi.org/10.20868/UPM.thesis.47779. (in Spanish)

Pechmann JC, Nava SJ, Terra FM, Bernier JC (2007) Local magnitude determination for intermountain seismic belt earthquakes from broadband digital data. Bull Seism Soc Am 97:557–574. https://doi.org/10.1785/0120060114

Prudencio J, Del Pezzo E, García-Yeguas A, Ibáñez JM (2013) Spatial distribution of intrinsic and scattering seismic attenuation in

active volcanic islands, I: model and the case of Tenerife Island. Geophys J Int 195:1942–1956. https://doi.org/10.1093/gji/ggt361

Richter CF (1935) An instrumental earthquake magnitude scale. Bull Seism Soc Am 25:1–32. https://doi.org/10.1785/BSSA0250010001

Richter CF (1958) Elementary seismology. W. H. Freeman and Co., San Francisco, p 578

Ristau J, Harte D, Salichon J (2016) A revised local magnitude (M$_L$) scale for New Zealand earthquakes. Bull Seism Soc Am 106:398–407. https://doi.org/10.1785/0120150293

Rueda J, Mezcua J (2005) Near-real-time seismic moment-tensor determination in Spain. Seism Res Lett 76:455–465. https://doi.org/10.1785/gssrl.76.4.455

Rueda J (coordinator), Abella R, Blanco MJ, Díaz EA, Domínguez IF, Domínguez J, Fernández de Villalta M, del Fresno C, López R, López C, López-Muga M, Muñoz A, Sánchez Sanz C, Mezcua J (2020) Revisión del Catálogo sísmico de las Islas Canarias (1341–2000). Centro Nacional de Información Geográfica, 230 pp. https://doi.org/10.7419/162.34.2020. (in Spanish)

Savage MK, Anderson JG (1995) A local-magnitude scale for the western Great Basin-eastern Sierra Nevada from synthetic Wood-Anderson seismograms. Bull Seismol Soc Am 85:1236–1243

Scordilis E, Kementzetzidou D, Papazachos B (2013) Local magnitude estimation in Greece, based on recording of the Hellenic Unified Seismic network (HUSN). Bull Geol Soc Greece 47:1241–1250. https://doi.org/10.12681/bgsg.10980

Uhrhammer RA, Collins ER (1990) Synthesis of Wood-Anderson seismograms from broadband digital records. Bull Seismol Soc Am 80:702–716

Uhrhammer RA, Loper SJ, Romanowicz B (1996) Determination of local magnitude using BDSN broadband records. Bull Seism Soc Am 86:1314–1330

Veith KF, Clawson GE (1972) Magnitude from short-period P-wave data. Bull Seismol Soc Am 99:554–565

Wyss M, Klein F, Nagamine K, Wiemer S (2001) Anomalously high b-values in the South Flank of Kilauea volcano, Hawaii: evidence for the distribution of magma below Kilauea's East rift zone. J Volc Geotherm Res 106:23–37. https://doi.org/10.1016/S0377-0273(00)00263-8

Yenier E (2017) A local magnitude relation for earthquakes in the western Canada sedimentary basin. Bull Seismol Soc Am 107:1421–1431. https://doi.org/10.1785/0120160275